

Observation of Geometric Heat Pump Effect in Periodic Driven Thermal Diffusion

Zi Wang,^{*} Jiangzhi Chen,^{*} Zhe Liu, and Jie Ren[†]

*Center for Phononics and Thermal Energy Science, China-EU Joint Lab on Nanophononics,
Shanghai Key Laboratory of Special Artificial Microstructure Materials and Technology,
School of Physics Science and Engineering, Tongji University, Shanghai 200092, China*

(Dated: January 23, 2022)

The concept of geometry works as an overarching framework underlying a wide range of transport phenomena. Particularly, the geometric phase effect in classical and quantum heat pump has been attracting much attention in microscopic systems. Here, we formulate theoretically the geometric heat pump effect in macroscopic driven diffusive systems. Upon modulation protocols, the nontrivial geometric curvature in the parameter space universally induces an additional pumped heat, beyond the constraint of hot-to-cold flowing. Furthermore, we set up a minimum experiment and indeed observe a non-vanishing directional heat flow across the driven system, despite keeping zero thermal bias between two time-dependent thermal reservoirs at every instant. We verify that in analogy to the geometric phase effect, the geometric pumped heat during each driving cycle is independent of driving periods in the adiabatic limit and coincides with theoretical predictions, thus validating its geometric origin. These results about geometric heat pump effect could have potential implications for designing and implementing nonreciprocal and topological thermal meta-devices under spatiotemporal modulations.

Introduction.— Recently the phononic thermal transport [1, 2] including the search for functional thermal devices, such as thermal diodes [3, 4], thermal transistors [5, 6], etc., raises a surge of interest, which is not only fundamentally central within the topics in nonequilibrium statistical physics [7–9], but also pragmatically promises the next generation thermal computation and thermal energy control. Furthermore, a series of spatially constructed thermal metamaterials and meta-devices [10, 11] have also been proposed to delicately regulate the heat flow direction and magnitude.

Nevertheless, in static macroscopic configurations, heat always flows globally from hot sources to cold drains therein, as dictated by the second law of thermodynamics. To circumvent this constraint, people resort to temporal drivings, which have already been applied to generate non-trivial Floquet states both in closed [12, 13] and open [14, 15] quantum systems. Meanwhile, temporal drivings have been introduced to thermal manipulations, producing novel theoretical effects like the directional heat flow in unbiased thermal transport [16, 17], periodically driven heat engines [18], non-reciprocal thermal metamaterials [19], dynamic photonic refrigeration [20], radiative heat shuttling [21], adiabatic thermal radiation pump [22], etc., as well as experimental observations, such as high-performance solid-state electrocaloric cooling [23], thermal non-Hermitian [24] and topological [25] dynamics, etc. These works explicitly demonstrate the power and versatility of temporal driving methods in thermal manipulation.

Considering the convenience brought by driving, it is demanding to grasp underlying universal concepts. The geometry emerges as one of the most insightful ideas. The geometric phase is originally proposed in closed quantum systems [26, 27], later generalized to the scattering process in open quantum systems [28] and also to the full counting statistics [29] in stochastic pump systems [30, 31] as an additional term obtained after a periodical modulation. Concerning the heat transport process, a similar geometric effect is unveiled in

an anharmonic quantum junction [32], which induces an additional pumped heat from cold to hot after one periodic driving, so called geometric heat pump. Subsequently, the geometric heat pump effect raises a plethora of research on its manifestation in nano-sized open quantum [33–35] and classical coupled oscillators [36]. Also, recently the connections with the entropy production [37], heat engines [38–40] and nonadiabatic control methods [41, 42] are established. These works emphasize the central status of the geometric heat pump [43].

Despite its massive theoretical attention and broad implications, the geometric heat pump effect has not been realized experimentally yet. Also, the geometric heat pump effect seems restricted to quantum nano-scale and microscopic stochastic systems, which brings the challenge obstructing the experimental verification. Therefore, a question naturally arises that whether the geometric heat pump effect is present in macroscopic diffusive systems. If so, how can the corresponding effect be experimentally observed and utilized to construct practical thermal devices?

In this Letter, we draw a positive conclusion on above questions. We excavate the geometric heat contribution in addition to the conventional dynamic heat flow in general driven diffusive systems, incorporating the situations of both continuous and discrete driving protocols, as shown in Fig. 1. We further elaborate a periodic driven experimental setup with reservoirs' temperature and thermal conductance modulated to demonstrate the geometric heat pump effect in the macroscopic thermal diffusion. The experimental observation verifies that a non-zero geometric heat flow is generated even under instantaneous zero bias at every instant. Meanwhile, the integrated heat contribution over each single driving period in the adiabatic limit (long driving period) is independent of the driving period, clearly validates our theoretical geometric formulation.

Geometric Heat Pump Effect.—We begin by recapitulating the well-known classical thermal diffusion, governed by the Fourier's law [44] $\mathbf{J} = -\kappa \nabla T(x, t)$ and the continuity equa-

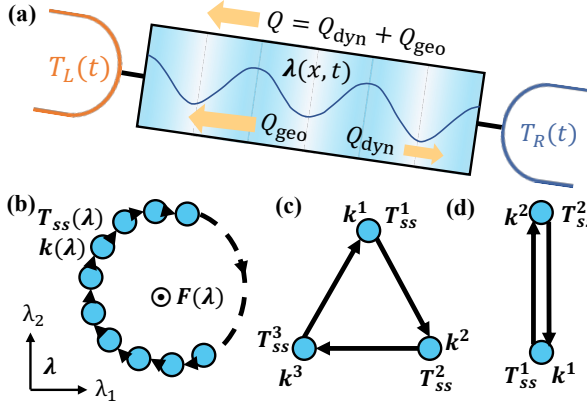


FIG. 1. A diagram of the geometry in driven diffusive systems from trotterized continuous protocols to discrete protocol.

(a) The heat transport as a competition between Q_{geo} and Q_{dyn} . The dynamic heat Q_{dyn} is always parallel to the temperature bias $T_L(t) - T_R(t)$, but Q can be against the bias, if the geometric heat Q_{geo} is dominant. (b) The trotterized continuous driving path. Filled dots $\lambda \equiv (\lambda_1, \lambda_2)$ denote points in the parameter space. Q_{geo} is induced by the intrinsic nontrivial curvature $F(\lambda)$. Both instantaneous steady state temperature \mathbf{T}_{ss} and dual \mathbf{k} are defined locally. (c) The multiple-point protocol defined by trotterizing the continuous protocol. The inner product between \mathbf{k}^n and $\Delta T_{ss}^n \equiv T_{ss}^n - T_{ss}^{n-1}$ quantifies geometric contribution during relaxation from steady state at point $n-1$ to that at n , wherein the systems' parameters are fixed at λ^n . (d) The two-point switching model. It corresponds to our experimental setup.

tion $\frac{\partial}{\partial t} E = -\nabla \cdot \mathbf{J}$. The Fourier's law states that the heat current density \mathbf{J} is proportional to the conductivity κ and inverse temperature gradient, while the continuity condition simply accounts for the energy conservation.

Spatially discretizing the central system with temperature vector \mathbf{T}_c and take into account the boundary temperature vector \mathbf{T}_b fixed by the connected reservoirs, the heat flow during the linear conduction process is given by the discrete Fourier's law: $\mathbf{J} = \mathcal{K}_c \mathbf{T}_c + \mathcal{K}_b \mathbf{T}_b$, where the conduction matrix \mathcal{K}_c (\mathcal{K}_b) depicts the conduction effect induced within system itself (by coupling to thermal reservoirs). The heat flow \mathbf{J} is a column vector containing currents between different neighbouring space points in the whole system. Considering the continuity relation governed by the energy conservation, the heat flow incurs the temperature evolution as $\frac{\partial}{\partial t} \mathbf{T}_c = \mathcal{L} \mathbf{J}$. Here, $\mathcal{L} \equiv \mathcal{C}^{-1} \mathcal{D}$. The diagonal matrix \mathcal{C} contains the heat capacity as its elements and \mathcal{D} is the divergence matrix (the discrete version of divergence operator $\nabla \cdot$). Their concrete form is exemplified in the section 1 of supplement [45].

Therefore, by combining the above two equations, the evolution of the system's temperature distribution is described by

$$\frac{\partial}{\partial t} \mathbf{T}_c = \mathcal{M}_c \mathbf{T}_c + \mathcal{M}_b \mathbf{T}_b, \quad (1)$$

where $\mathcal{M}_c \equiv \mathcal{L} \mathcal{K}_c$ and $\mathcal{M}_b \equiv \mathcal{L} \mathcal{K}_b$. The invertible matrix \mathcal{M}_c describes the cooling process of the central system if the reservoirs are set to the zero temperature. The above abstract

notions are exemplified by a concrete one dimensional model (See section 1 in supplement [45]) to clarify the physical implication.

In the adiabatic limit, the driving is slow enough for the system to relax to its instantaneous steady state at every instant. According to the adiabatic perturbation theory [46], $\partial \mathbf{T}_c / \partial t$ can be considered as a perturbation term. To the zeroth order, the steady state of \mathbf{T}_c is obviously $\mathbf{T}_{ss} = -(\mathcal{M}_c)^{-1} \mathcal{M}_b \mathbf{T}_b$. This is the exact result of $\mathbf{T}_c(t)$ if no driving is applied. To the first order of driving speed, adiabatic perturbation (as shown in the section 2 of the supplement [45]) yields the separation of heat flow into the dynamic and geometric components

$$J_{\text{dyn}} = \mathbf{1} \cdot \mathcal{K}_c \mathbf{T}_{ss} + \mathbf{1} \cdot \mathcal{K}_b \mathbf{T}_b, \quad (2)$$

$$J_{\text{geo}} = \mathbf{k} \cdot \frac{\partial \mathbf{T}_{ss}}{\partial \lambda_i} \dot{\lambda}_i, \quad (3)$$

where we adopt the convention of summing repeated indices. The vector $\mathbf{k} \equiv \mathbf{1} \cdot \mathcal{K}_c (\mathcal{M}_c)^{-1}$ is a row vector mapping the variation speed of \mathbf{T}_{ss} into heat current components. It is in the dual space of \mathbf{T}_{ss} and is reminiscent of the quantum “bra”. $\mathbf{1}$ is a row vector whose components are zero except $1_i = 1$, with i denoting our interested current component. λ is the vector of driven parameters. The dynamic part is simply a steady state current in static situation. The geometric contribution J_{geo} has no analogy in static systems.

Suppose the parameters of the system are driven cyclically, the accumulative geometric heat flow during one single period is

$$Q_{\text{geo}} \equiv \int_0^{\tau_p} J_{\text{geo}}(t) dt = \oint_{\partial \Omega} d\lambda \cdot \mathbf{A}. \quad (4)$$

Here, the geometric connection independent of the driving speed is $\mathbf{A} \equiv \mathbf{k} \cdot \nabla_{\lambda} \mathbf{T}_{ss}$, with $\partial \Omega$ being the closed protocol path. It is reminiscent of the original Berry connection [26] and similar counterparts in microscopic stochastic systems [32]. The protocol can be parametrized as $\{\lambda(t)\}_{0 \leq t < \tau_p}$, where τ_p is the driving period.

In the situation where two parameters are modulated, i.e., $\lambda = (\lambda_1, \lambda_2)^T$, Q_{geo} is also formulated as, with the aid of the Stokes formula,

$$Q_{\text{geo}} = \int_{\Omega} F(\lambda) d\Omega, \quad (5)$$

$$F(\lambda) \equiv \frac{\partial \mathbf{k}}{\partial \lambda_1} \cdot \frac{\partial \mathbf{T}_{ss}}{\partial \lambda_2} - \frac{\partial \mathbf{k}}{\partial \lambda_2} \cdot \frac{\partial \mathbf{T}_{ss}}{\partial \lambda_1}.$$

The curvature $F(\lambda)$ is the geometric curvature and the integration is over the area Ω encircled by the closed path $\partial \Omega$. $d\Omega$ is the corresponding surface element. The intrinsic nontrivial curvature $F(\lambda)$ induces the accumulated pumped heat in each period, independent of τ_p .

Switching Driving Protocol.—A continuous driving protocol can be trotterized into a discrete one. Here we discuss the crossover from continuous drivings to protocols where system

parameters are just switched back and forth between several states. Accordingly, the dynamic and geometric components of the accumulated pumped heat as integrals are replaced by corresponding summations

$$Q_{\text{dyn}} = \sum_{n=1}^N (1 \cdot \mathcal{K}_c^n \mathbf{T}_{ss}^n + 1 \cdot \mathcal{K}_b^n \mathbf{T}_b^n) \frac{\tau_p}{N}, \quad (6)$$

$$Q_{\text{geo}} = \sum_{n=1}^N \mathbf{k}^n \cdot \Delta \mathbf{T}_{ss}^n. \quad (7)$$

Q_{geo} has a nature comparable with the original Pancharatnam geometric phase [47], but here in a non-Hermitian sense. We trotterize the protocol into N pieces, with system parameters being constant within each τ_p/N duration. \mathcal{K}_c^n , \mathcal{K}_b^n and \mathbf{k}^n correspond to the system parameters in the n -th protocol piece. After each quench of system parameters, the system relaxes and dissipates. Considering the adiabaticity of driving, the system temperature relaxes to its steady state at the end of each driving piece. \mathbf{T}_{ss}^n is the system temperature after finishing the n -th piece and right before the next quench. Also, \mathbf{T}_{ss}^n is calculated to be $\mathbf{T}_{ss}^n \equiv -(\mathcal{M}_c^n)^{-1} \mathcal{M}_b^n \mathbf{T}_b^n$, identical to the adiabatic steady state in the continuous driving situation. In Eq. (7), the difference between two adjacent steady states is defined as $\Delta \mathbf{T}_{ss}^n \equiv \mathbf{T}_{ss}^n - \mathbf{T}_{ss}^{n-1}$. For the details of a direct derivation, see section 2 in supplement [45].

As a limit case, also in alignment with the experiment carried out and shown below, the geometrically pumped heat is simplified to be

$$Q_{\text{geo}} = (\mathbf{k}^1 - \mathbf{k}^2) \cdot (\mathbf{T}_{ss}^1 - \mathbf{T}_{ss}^2), \quad (8)$$

if the system parameters are cyclically switched between only two states. This is apparently independent of τ_p , justifying its geometric origin. The above result encapsulates a non-zero directional heat flow arising solely from the driving even when no instantaneous non-zero thermal bias is introduced. This phenomenon is observed in our experiment. A unified geometric perspective of continuous and discrete protocols is schematically shown in Fig. 1.

Experimental Demonstration.—To observe the geometric heat pump, we start with a typical structure as described in Fig. 2(a). We connect both ends of the copper plate to the thermal reservoirs with identical temperatures T_b . The thermal conductance between the copper plate and two reservoirs, i.e. κ_1 and κ_2 , are out of phase. In Fig. 2(b), we show the periodic protocols of T_b , κ_1 and κ_2 . We demonstrate the two possible system configurations in Fig. 2(c). In configuration I, the thermal reservoirs are at high temperature, and the copper plate is only connected to the left thermal reservoirs. The thermal conductance on the left equals its maximum value κ . From I to II, we instantaneously switch the temperature of reservoirs from T_{hot} to T_{cold} . Meanwhile, the central system is connected to the right reservoir and disconnected from the left one.

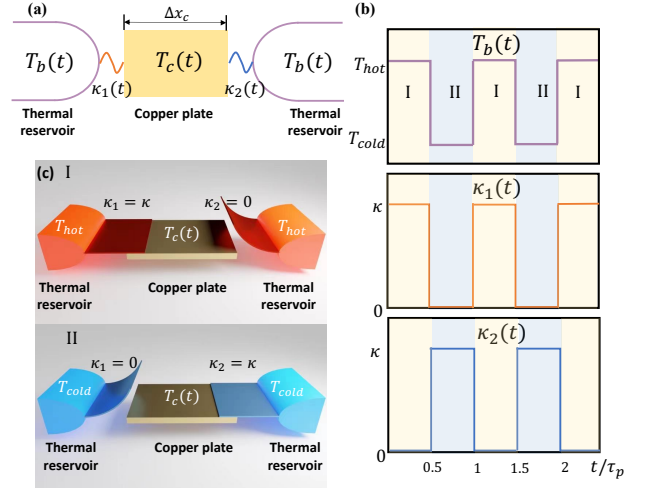


FIG. 2. **The schematic diagram of the experimental setup and the driving protocol.** (a) The central system (the copper plate) is coupled to two thermal reservoirs with identical temperature. The temperature of the copper plate is T_c and that of reservoirs is T_b . The two thermal conductances between the copper plate and reservoirs are κ_n ($n = 1, 2$) with a maximum κ . T_c , T_b and κ_n change over time. Δx_c is the width of the copper plate. (b) The temporal modulation of the reservoirs' temperature T_b and conductance κ_n with τ_p being the driving period. The system parameters are switched instantaneously between state I and II. (c) The corresponding system configurations in two parameter states (I and II). The conductance modulation is controlled by the SMA.

To modulate κ_1 and κ_2 in the experiment, we construct the system-reservoir couplings with two types of reversible shape memory alloys (SMA). The geometric configurations of SMA change rapidly as its temperature varies, which is also applied in macroscopic thermal diodes [48]. When the thermal reservoirs are at T_{hot} , the SMA-1 is flat and the SMA-2 is warped, and when the reservoirs are switched to T_{cold} , the configurations of two SMAs are reversed. Therefore, the switching of reservoirs spontaneously induces the modulation of κ_1 and κ_2 , through the mechanical response of SMAs.

Figure 3(a) is an infrared imaging snapshot of Fig. 2(a). The copper plate (with a width of $\Delta x_c = 50\text{mm}$) is coupled to two thermal reservoirs with heat capacity much greater than that of the plate. The SMAs are much thinner than the copper plate (see section 3 in supplement [45] for more details of the setup), rendering its capacity negligible. The thermal conductance κ_n in our experiment is not necessarily used for analysis, due to the presence of dissipation into the surrounding atmosphere. Thus, we calibrate the effective conductances σ_n instead of κ_n in the experiment. We couple the copper plate to one side of thermal reservoir at a time and record the time dependence of T_c . $\sigma = 0.049\text{ W/K}$ is obtained from the mean relaxation time (see more discussions in section 4 of supplement [45]). We also calibrate the maximum and minimum temperature of the effective thermal reservoir T_e as $T_{\text{hot}} = 35.2^\circ\text{C}$ and $T_{\text{cold}} = 14.8^\circ\text{C}$ (section 4 of supple-

ment [45]).

According to the theory, we analytically calculate the heat transferred during one single period as

$$Q = C\Delta T_e(1 - e^{-\frac{\sigma\tau_p}{2C}}), \quad (9)$$

where C is the heat capacity of the central system, $\Delta T_e \equiv T_{\text{hot}} - T_{\text{cold}}$ (more details in section 5 of supplement [45]). In our experimental setup, $C=26.208$ J/K and $\Delta T_e=20.4^\circ\text{C}$. In spite of the driving frequency, the dynamical component of the transferred heat during one single period is $Q_{\text{dyn}} \equiv 0$ due to the strict instantaneous zero bias of the thermal reservoirs. The pumped heat is singly contributed to Q_{geo} .

In the adiabatic limit ($\tau_p \rightarrow \infty$), Eq. (9) reduces to

$$Q = C\Delta T_e. \quad (10)$$

To form a connection with our general theory, we note that steady states $\mathbf{T}_{ss}^n := T_b^n$ ($n=\text{I, II}$). Also, defining the positive direction of the current as left to right, $\mathcal{M}_c^n := -(\sigma_1^n + \sigma_2^n)/C$ and $\mathcal{K}_c^n := (-\sigma_1^n, \sigma_2^n)^T$. Without losing any generality, we select $\mathbf{1} := (1, 0)^T$. Thus, $\mathbf{k}^1 - \mathbf{k}^2 = C$ and Eq. (8) reduces to $Q_{\text{geo}} = C\Delta T_e$, in agreement with Eq. (10), showing Q in our experiment to be purely geometric. The details of this compare is given in the section 5 of supplement [45]. Also, the measured result of Eq. (10) is shown in Fig. 3(b).

Figure 3(b)(c) shows results of our observation and measurement of the geometric heat pump effect. We record the temperature evolution of the copper plate $T_c(t)$ under different driving period τ_p . After several periods, the system enters a periodic state. Then we measure the heat transferred during one single period under different driving periods τ_p , which is displayed in Fig. 3(b). The black line shows the theoretical value from Eq. (9) and the dots show the experimental results. In the fast driving region, Q and τ_p are approximately linearly correlated, consistent with $Q \approx \frac{\sigma\Delta T_e}{2}\tau_p$. In the adiabatic limit ($\tau_p \gg \tau_c \equiv 2C/\sigma$), Q remains unchanged as τ_p varies, and its experimental plateau value $Q_{\text{geo}} = 545\text{J}$ agrees with the theoretical value $Q_{\text{geo}} = 535\text{J}$ predicted by Eq. (10). This proves the existence of general geometric heat pump effects in the classical diffusive transport.

To further analyze the pump process, Fig. 3(c) shows the variations of the copper plate's temperature T_c in different driving periods τ_p , representing the two cases—the fast driving (yellow background) and slow driving (green background) regimes. In the case of fast driving ($\tau_p=240$ s), T_c reciprocates in a small interval due to the system's being impossible to respond instantaneously. As τ_p increases to 1920s, the difference of T_c in a period gets larger. Within the adiabatic regime ($\tau_p=10800$ s), the maximum (minimum) value of $T_c(t)$ is equal to T_{hot} (T_{cold}). Compared with the instantaneous change of the thermal reservoirs, the delay of T_c owes to the finite relaxation time of thermal diffusion.

In the adiabatic limit ($\tau_p=10800$ s), the thermodynamic process is formed of four phases in one period, which are marked as ①, ②, ③, ④ in Fig. 3(d). We display the details of the four phases with infrared imaging snapshots in Fig. 3(e). From

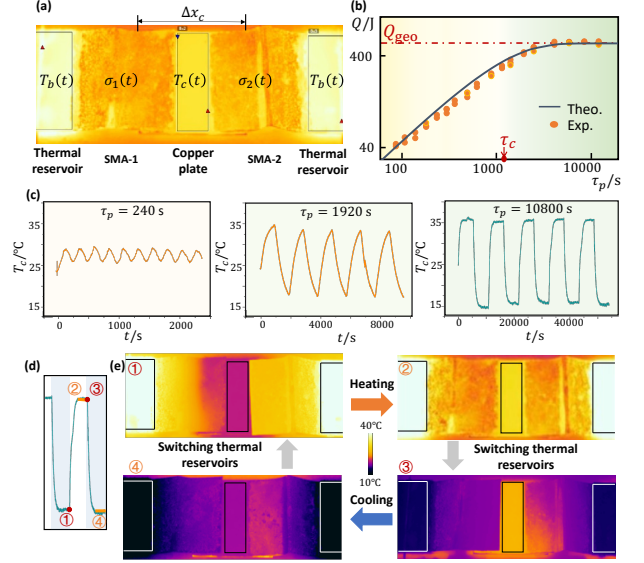


FIG. 3. The observation of the geometric heat pump in the thermal diffusion system. (a) A snapshot of the experimental device generated by an infrared thermal imager, corresponding to Fig. 2. (b) The heat transferred during a single driving period versus different τ_p . The characteristic time $\tau_c \equiv 2C/\sigma=1070$ s signifies the crossover between two regimes—fast driving and slow driving, marked by the yellow and green background color, respectively. The geometric heat pump effect is observed as the plateau $Q_{\text{geo}}=546\text{J}$ when the driving is slow. (c) The evolution of T_c in different τ_p situations, corresponding to the fast, intermediate, and fast driving cases in (b). The maximum and minimum of T_c get closer to that of the thermal reservoirs as τ_p gets longer. (d) A typical period in the evolution of T_c ($\tau_p=10800$ s), which contains four phases. The background colors distinguish the different parameter states. (e) Snapshots of the experiment device in the four phases in the adiabatic limit. The four phases correspond to ①, ②, ③ and ④ in (d), respectively.

phase ① to ②, the central system is coupled to the left hot thermal reservoir. Heat flows from left reservoir to the central system. After switching the two hot thermal reservoirs to cold ones, the central system only connects with the right reservoir. Heat flows from the central system to the right thermal reservoir (phase ③ to ④). Thus, there is a one-way heat flow in the device. This thermodynamic cycle analysis provides an intuitive picture of the geometric heat pump effect. Since the central system is always isolated with one of the reservoirs, the pumping can be unambiguously traced to the difference of central system's two steady states, which equates ΔT_e . The corresponding absorbing from the left (draining into the right) incurs the central system's energy change [Eq. (10)] from phase ① to ② (③ to ④). This energy change is evidently the pumped heat during the whole cycle and independent of the adiabatic driving period. This attributes the physical picture of the geometrically pumped heat, i.e. Eq. (5)(7)(8), to the changing of system states, which originates to the intrinsic geometric properties of the parameter space.

Conclusion.—To summarize, we have unveiled the intrinsic

sic geometry underlying the driven diffusive thermal conduction process through both theoretical formulation and experimental observation. The experimental result in the adiabatic limit is well described by our derived general theoretical results. Our work, by unambiguous observation of the geometric heat flow, paves the way for future generalization to more complex systems. This would enable a versatile and reliable resource in generating directional heat flow and harnessing thermal energy by devising a dynamical toolkit. Constructing geometric effect induced non-reciprocal and topological phenomena [19, 49] in driven diffusive processes constitutes a promising task.

Acknowledgments. We acknowledge the support from the National Natural Science Foundation of China (Nos. 11935010 and 11775159), and the Opening Project of Shanghai Key Laboratory of Special Artificial Microstructure Materials and Technology.

* These two authors contributed equally to this work.

† Corresponding Email: Xonics@tongji.edu.cn

- [1] Abhishek Dhar, “Heat transport in low-dimensional systems,” *Adv. Phys.* **57**, 457–537 (2008).
- [2] Nianbei Li, Jie Ren, Lei Wang, Gang Zhang, Peter Hänggi, and Baowen Li, “Colloquium: Phononics: Manipulating heat flow with electronic analogs and beyond,” *Rev. Mod. Phys.* **84**, 1045–1066 (2012).
- [3] Baowen Li, Lei Wang, and Giulio Casati, “Thermal diode: Rectification of heat flux,” *Phys. Rev. Lett.* **93**, 184301 (2004).
- [4] Chih Wei Chang, D Okawa, A Majumdar, and A Zettl, “Solid-state thermal rectifier,” *Science* **314**, 1121–1124 (2006).
- [5] Philippe Ben-Abdallah and Svend-Age Biehs, “Near-field thermal transistor,” *Phys. Rev. Lett.* **112**, 044301 (2014).
- [6] Karl Joulain, Jérémie Drevillon, Younès Ezzahri, and Jose Ordóñez-Miranda, “Quantum thermal transistor,” *Phys. Rev. Lett.* **116**, 200601 (2016).
- [7] Keiji Saito and Abhishek Dhar, “Fluctuation theorem in quantum heat conduction,” *Phys. Rev. Lett.* **99**, 180601 (2007).
- [8] Sushant Saryal, Hava Meira Friedman, Dvira Segal, and Bijay Kumar Agarwalla, “Thermodynamic uncertainty relation in thermal transport,” *Phys. Rev. E* **100**, 042101 (2019).
- [9] Peter Talkner and Peter Hänggi, “Colloquium: Statistical mechanics and thermodynamics at strong coupling: Quantum and classical,” *Rev. Mod. Phys.* **92**, 041002 (2020).
- [10] Shuai Yang, Jun Wang, Gaole Dai, Fubao Yang, and Jiping Huang, “Controlling macroscopic heat transfer with thermal metamaterials: Theory, experiment and application,” *Phys. Rep.* **908**, 1–65 (2021).
- [11] Ying Li, Wei Li, Tiancheng Han, Xu Zheng, Jiabin Li, Baowen Li, Shanhui Fan, and Cheng-Wei Qiu, “Transforming heat transfer with thermal metamaterials and devices,” *Nat. Rev. Mater.* **6**, 488–507 (2021).
- [12] Takuya Kitagawa, Erez Berg, Mark Rudner, and Eugene Demler, “Topological characterization of periodically driven quantum systems,” *Phys. Rev. B* **82**, 235114 (2010).
- [13] Wenchao Ma, Longwen Zhou, Qi Zhang, Min Li, Chunyang Cheng, Jianpei Geng, Xing Rong, Fazhan Shi, Jiangbin Gong, and Jiangfeng Du, “Experimental observation of a generalized thouless pump with a single spin,” *Phys. Rev. Lett.* **120**, 120501 (2018).
- [14] Georg Engelhardt, Gloria Platero, and Jianshu Cao, “Discontinuities in driven spin-boson systems due to coherent destruction of tunneling: Breakdown of the floquet-gibbs distribution,” *Phys. Rev. Lett.* **123**, 120602 (2019).
- [15] Georg Engelhardt and Jianshu Cao, “Dynamical symmetries and symmetry-protected selection rules in periodically driven quantum systems,” *Phys. Rev. Lett.* **126**, 090601 (2021).
- [16] Nianbei Li, Peter Hänggi, and Baowen Li, “Ratcheting heat flux against a thermal bias,” *EPL* **84**, 40009 (2008).
- [17] Jie Ren and Baowen Li, “Emergence and control of heat current from strict zero thermal bias,” *Phys. Rev. E* **81**, 021111 (2010).
- [18] Rahul Marathe, A. M. Jayannavar, and Abhishek Dhar, “Two simple models of classical heat pumps,” *Phys. Rev. E* **75**, 030103 (2007).
- [19] Daniel Torrent, Olivier Poncelet, and Jean-Christophe Bat-sale, “Nonreciprocal thermal material by spatiotemporal modulation,” *Phys. Rev. Lett.* **120**, 125501 (2018).
- [20] Siddharth Buddhiraju, Wei Li, and Shanhui Fan, “Photonic refrigeration from time-modulated thermal emission,” *Phys. Rev. Lett.* **124**, 077402 (2020).
- [21] Ivan Latella, Riccardo Messina, J. Miguel Rubi, and Philippe Ben-Abdallah, “Radiative heat shuttling,” *Phys. Rev. Lett.* **121**, 023903 (2018).
- [22] Huanan Li, Lucas J. Fernández-Alcázar, Fred Ellis, Boris Shapiro, and Tsampikos Kottos, “Adiabatic thermal radiation pumps for thermal photonics,” *Phys. Rev. Lett.* **123**, 165901 (2019).
- [23] Yunda Wang, Ziyang Zhang, Tomoyasu Usui, Michael Benedict, Sakyo Hirose, Joseph Lee, Jamie Kalb, and David Schwartz, “A high-performance solid-state electrocaloric cooling system,” *Science* **370**, 129–133 (2020).
- [24] Ying Li, Yu-Gui Peng, Lei Han, Mohammad-Ali Miri, Wei Li, Meng Xiao, Xue-Feng Zhu, Jianlin Zhao, Andrea Alù, Shanhui Fan, *et al.*, “Anti-parity-time symmetry in diffusive systems,” *Science* **364**, 170–173 (2019).
- [25] Guoqiang Xu, Ying Li, Wei Li, Shanhui Fan, and Cheng-Wei Qiu, “Configurable phase transitions in a topological thermal material,” *Phys. Rev. Lett.* **127**, 105901 (2021).
- [26] Michael Victor Berry, “Quantal phase factors accompanying adiabatic changes,” *Proc. R. Soc. A* **392**, 45–57 (1984).
- [27] D. J. Thouless, “Quantization of particle transport,” *Phys. Rev. B* **27**, 6083–6087 (1983).
- [28] P. W. Brouwer, “Scattering approach to parametric pumping,” *Phys. Rev. B* **58**, R10135–R10138 (1998).
- [29] N. A. Sinitsyn and Ilya Nemenman, “Universal geometric theory of mesoscopic stochastic pumps and reversible ratchets,” *Phys. Rev. Lett.* **99**, 220408 (2007).
- [30] R Dean Astumian and Peter Hänggi, “Brownian motors,” *Phys. Today* **55**, 33 (2002).
- [31] Saar Rahav, Jordan Horowitz, and Christopher Jarzynski, “Directed flow in nonadiabatic stochastic pumps,” *Phys. Rev. Lett.* **101**, 140602 (2008).
- [32] Jie Ren, Peter Hänggi, and Baowen Li, “Berry-phase-induced heat pumping and its impact on the fluctuation theorem,” *Phys. Rev. Lett.* **104**, 170601 (2010).
- [33] Tian Chen, Xiang-Bin Wang, and Jie Ren, “Dynamic control of quantum geometric heat flux in a nonequilibrium spin-boson model,” *Phys. Rev. B* **87**, 144303 (2013).
- [34] Chen Wang, Jie Ren, and Jianshu Cao, “Unifying quantum heat transfer in a nonequilibrium spin-boson model with full counting statistics,” *Phys. Rev. A* **95**, 023610 (2017).
- [35] Wenjie Nie, Guoyao Li, Xiyun Li, Aixi Chen, Yueheng Lan, and Shi-Yao Zhu, “Berry-phase-like effect of thermo-phonon

- transport in optomechanics,” *Phys. Rev. A* **102**, 043512 (2020).
- [36] Jie Ren, Sha Liu, and Baowen Li, “Geometric heat flux for classical thermal transport in interacting open systems,” *Phys. Rev. Lett.* **108**, 210603 (2012).
 - [37] Takahiro Sagawa and Hisao Hayakawa, “Geometrical expression of excess entropy production,” *Phys. Rev. E* **84**, 051110 (2011).
 - [38] Kay Brandner and Keiji Saito, “Thermodynamic geometry of microscopic heat engines,” *Phys. Rev. Lett.* **124**, 040602 (2020).
 - [39] Bibek Bhandari, Pablo Terrén Alonso, Fabio Taddei, Felix von Oppen, Rosario Fazio, and Liliana Arrachea, “Geometric properties of adiabatic quantum thermal machines,” *Phys. Rev. B* **102**, 155407 (2020).
 - [40] Yuki Hino and Hisao Hayakawa, “Geometrical formulation of adiabatic pumping as a heat engine,” *Phys. Rev. Research* **3**, 013187 (2021).
 - [41] Ken Funo, Neill Lambert, Franco Nori, and Christian Flindt, “Shortcuts to adiabatic pumping in classical stochastic systems,” *Phys. Rev. Lett.* **124**, 150603 (2020).
 - [42] Kazutaka Takahashi, Keisuke Fujii, Yuki Hino, and Hisao Hayakawa, “Nonadiabatic control of geometric pumping,” *Phys. Rev. Lett.* **124**, 150602 (2020).
 - [43] Zi Wang, Luqin Wang, Jiangzhi Chen, Chen Wang, and Jie Ren, “Geometric heat pump: Controlling thermal transport with time-dependent modulations,” *Front. Phys.* **17**, 1–14 (2022).
 - [44] Herbert B Callen, *Thermodynamics and an Introduction to Thermostatistics* (Wiley, New York, 1985).
 - [45] Supplementary Material.
 - [46] Michael Kolodrubetz, Dries Sels, Pankaj Mehta, and Anatoli Polkovnikov, “Geometry and non-adiabatic response in quantum and classical systems,” *Phys. Rep.* **697**, 1–87 (2017).
 - [47] Shivaramakrishnan Pancharatnam, “Generalized theory of interference and its applications,” *Proc. Indian Acad. Sci. A*, **44**, 398–417 (1956).
 - [48] Ying Li, Xiangying Shen, Zuhui Wu, Junying Huang, Yixuan Chen, Yushan Ni, and Jiping Huang, “Temperature-dependent transformation thermotics: From switchable thermal cloaks to macroscopic thermal diodes,” *Phys. Rev. Lett.* **115**, 195503 (2015).
 - [49] Lucas J. Fernández-Alcázar, Rodion Kononchuk, Huanan Li, and Tsampikos Kottos, “Extreme nonreciprocal near-field thermal radiation via floquet photonics,” *Phys. Rev. Lett.* **126**, 204101 (2021).